

Chaotic self-similar wave maps coupled to gravity

Sebastian J. Szybka

Institute of Physics, Jagellonian University, Kraków, Poland

Institute for Theoretical Physics, University of Vienna, Vienna, Austria*

November 10, 2018

Abstract

We continue our studies of spherically symmetric self-similar solutions in the $SU(2)$ sigma model coupled to gravity. For some values of the coupling constant we present numerical evidence for the chaotic solution and the fractal threshold behavior. We explain this phenomenon in terms of horseshoe-like dynamics and heteroclinic intersections.

1 Introduction

This is the fourth paper in a series aimed at understanding of the structure of the self-similar spherically symmetric wave maps coupled to gravity. In the first two papers [1, 2] it was shown that for the coupling constant $\alpha < \frac{1}{2}$ there exists a countable family of solutions that are analytic below the past light cone of the central singularity. It was also shown that there are two generic types of solutions beyond the past light cone. The threshold between these two generic types resembles many aspects of critical phenomenon and has been studied in [3] for the coupling constant $\alpha < 0.426$. It was found that for this coupling the threshold solutions are the periodic solutions. Now, we extend studies of the threshold solutions for larger coupling constant and examine the structure of the bifurcations in this parameter. This article is mathematically self-contained but for physical background we refer the reader to [1, 4].

2 Setting the problem

Under the assumption of spherical symmetry and self-similarity the Einstein's equations with wave map matter reduce to a system of autonomous equations [1]

*preprint no. UWThPh-2003-29

$$W' = -1 + \alpha(1 - W^2)F'^2, \quad (1)$$

$$A' = -2\alpha AW F'^2, \quad (2)$$

$$(AF')' = \frac{\sin(2F)}{W^2 - 1}, \quad (3)$$

subject to the constraint

$$1 - A - 2\alpha \sin^2(F) + \alpha AF'^2(W^2 - 1) = 0. \quad (4)$$

Physically the functions W and A parameterize the metric and the function F parameterizes the corotational wave map. α stands for a dimensionless coupling constant ($\alpha = 0$ corresponds to no gravity). We are interested in solutions of (1-4) starting at x_0 (we choose $x_0 = 0$) with the following initial conditions

$$W(0) = 1, \quad A(0) = 1 - 2\alpha, \quad F(0) = \frac{\pi}{2}, \quad F'(0) = b \quad (5)$$

where b is a free parameter (since the system has reflection symmetry $F \rightarrow -F$ we can take $b > 0$ without loss of generality). Solving (4) for A and using a new variable $D = F'$ we rewrite equations (1-3) as the three dimensional, autonomous, first order system ($\alpha < \frac{1}{2}$)

$$W' = -1 + \alpha(1 - W^2)D^2, \quad (6)$$

$$D' = 2\alpha W D^3 + \frac{\sin(2F)}{-1 + 2\alpha \sin^2(F)} \left(\alpha D^2 + \frac{1}{1 - W^2} \right), \quad (7)$$

$$F' = D. \quad (8)$$

with the initial conditions

$$W(0) = 1, \quad D(0) = b, \quad F(0) = \frac{\pi}{2}. \quad (9)$$

In the following we will refer to solutions of (6-8) satisfying the initial conditions (9) as b -orbits. It was shown in [2] that for $\alpha \in [0, \frac{1}{2})$ b -orbits exist locally and are analytic in b and x .

3 Types of solutions

It was shown in [1] that for small values of b the b -orbits exist up to the future light cone ($W = -1$) of central singularity, while for large values of b the b -orbits develop a sort of singular apparent horizon beyond which they cannot be continued ($W = +1$). These two types of solutions, call them type A and type B solutions, respectively, can be shown to form open sets [3]. Hence, there must exist solutions which are not type A or B, call them type C solutions. For a given α there exists a critical value $b^*(\alpha)$ such that solutions with $b < b^*$ are of type A, solutions with $b > b^*$ are of type B, and the solutions with $b = b^*$

is of type C; in other words, we have a bistable behavior with two generic final states A ($W = -1$) and B ($W = +1$), and the separatrix C ($|W| < 1$ for all x). We use the same terminology to distinguish attractors A ($W = -1$) and B ($W = +1$).

It was shown in [3] that type C solutions are asymptotically periodic for $\alpha < 0.426$. We will show in this paper that this remains valid for $\alpha > 0.482$. However, we will also show that for $\alpha \in (0.426, 0.482)$ (approximately) the transition between types A and B does not occur at a single point but in a narrow interval (b_{min}^*, b_{max}^*) and the behavior of type C solutions is chaotic. This chaotic behavior is the main point of our interest.

4 Type C solutions

Numerical data show that for general initial conditions the whole phase space contains two basin sets (of attractors A and B) separated by a two dimensional surface. Type C solutions lay in this critical surface. In other words all initial points in the critical surface give type C solutions. The critical surface is an invariant submanifold.

We are especially interested in asymptotic structure of type C solutions. Hereafter we will skip initial part of C solutions to simplify all figures. Let us call our asymptotic structure C-attractor. In fact, it is the attractor of codimension one (two stable and one unstable directions). The structure of C-attractor for $\alpha < 0.426$ has been found in [3] it is the periodic solution. In other words, b -orbits starting close to the critical b^* follow periodic C-attractor for some time and then run towards A or B attractor (see figure 1).

5 The bifurcation diagram

Let us consider the initial curve in the form (9). For each α , using the bisection procedure, we can find a critical values of b^* parameter which determine intersection of the initial curve with critical surface (figure 2). It has been noted in [1] that for large values of $\alpha \sim 0.43$, $b^*(\alpha)$ is not a single point but there is a structure hidden in a narrow interval ($b_{min}^*(\alpha), b_{max}^*(\alpha)$). The solutions here are sensitive to initial conditions infinitesimally small change of b parameter can result in a completely different final state. We have confirmed these numerical results. Since the magnitude of interval ($b_{min}^*(\alpha), b_{max}^*(\alpha)$) is of order 10^{-9} we used quadruple machine precision. In addition, the initial conditions (9) are given at a singular point. We are interested only in asymptotic structure of type C solutions so it is more convenient to reformulate initial curve to start directly from C-attractor

$$W(0) = 0, \quad D(0) = c, \quad F(0) = 0, \quad (10)$$

where c is a function of b such that $|c_{max}^* - c_{min}^*| \gg |b_{max}^* - b_{min}^*|$. The function $c(\alpha)$ is qualitatively similar to $b(\alpha)$ but now at α approximately equal to 0.426 we can resolve better the new structure in the diagram (figure 3). This

is a bifurcation point. Numerical results suggest that this new structure is self-similar (figures 3, 4, 5) so for each α we have infinitely many critical points. This suggests that the basin boundary is fractal.

There is not enough numerical data to calculate the fractal dimension from the definition but the phenomenon of fractal basin boundaries is well known so we have another tools to do this. We use the procedure suggested in [5] which goes as follows.

We call a point ϵ -uncertain if perturbations with $\epsilon \ll 1$ in opposite directions give points which belong to different basin sets. It was shown in [5] that the number of uncertain points in the phase space f scales as

$$f(\epsilon) \sim \epsilon^a. \quad (11)$$

Therefore, in the limit we have

$$\lim_{\epsilon \rightarrow 0} \frac{\ln f(\epsilon)}{\ln \epsilon} = a. \quad (12)$$

It was shown in [5] that the uncertainty exponent a is related to the capacity dimension d in D dimensional phase space by the formula

$$d = D - a. \quad (13)$$

For $\alpha = 0.4264$ we estimate numerically the capacity dimension to be $d = 0.337 \pm 0.003$ (see figure 6). Since C-attractor lays in critical surface with infinite area one should expect complicated dynamic. Figure 3 shows only one dimensional relation. It would be interesting to look at the whole basin boundary. We can do this by taking slices of the phase space (see figure 7).

6 C-attractor

We found C-attractor in this interval of α numerically (figures 8 and 9). The problem is not trivial because C-attractor lays in the unstable manifold (two stable and one unstable directions). We use straddle-orbit method due to Battelino et al. [6] and H. Nusse and J. Yorke [7].

This procedure allows us to pursue the unstable orbit laying in the basin boundary in principle forever. It can be viewed as a series of bisections and goes as follows. At initial time we choose two points $P_A(x=0)$ and $P_B(x=0)$ which lead to different attractors A and B and perform bisection until the distance between the iterates $P_A(0)$ and $P_B(0)$ is less a prescribed δ . Next we integrate the equations numerically starting from the current $P_A(0)$ and $P_B(0)$ until the distance between the trajectories exceeds δ . When this happens at some time x we stop the integration, assign the points $P_A(x)$ and $P_B(x)$ as current representatives and repeat the bisection. Iterating this procedure one can progressively construct a trajectory staying within a distance δ from the codimension one stable manifold.

Using straddle-orbit method we found two loops and a sequence of the windings (figure 10). It is in a way similar to the Lorenz attractor but the nature of C-attractor is different. The standard methods like Lyapunov exponents, test of the subsequent maxima, Poincaré sections of the attractor do not give good insight into the problem although behavior of maximal Lyapunov exponent indicate the chaotic region (see figure 7 in [3]). The best evidence of chaotic properties provides the autocorrelation function which exhibits a typical behavior (figure 11). It shows that we are able to predict short range behavior of the system (inside single loops) with good accuracy but long, deterministic sequence of windings is uncorrelated. We can show this numerically up to almost any finite period with help of the symbolic dynamics and information theory. Symbolization¹ allows us to check periodicity of our solutions, calculate Shannon entropy or EMC (Effective Measure of Complexity given by Grassberger [8]) and show sensitivity to initial conditions.

7 The horseshoe-like dynamics

The results presented in previous subsections are based on numerical calculations. It is well known that chaos and fractal structures could appear in dynamical systems due to the discretization errors [9]. In order to make confident that our result is not a numerical artifact we checked (in the bifurcation diagram) the dependence of the size of chaotic windows on machine precision. We have performed this calculation with positive result: the size of the chaotic windows does not tend to zero with increasing machine precision (figure 12). Unfortunately there is not enough computational efficiency to use more detailed lattice and estimate the limit.

In summary, we have strong numerical evidence for chaos but we need a qualitative argument. Here enters the horseshoe.

Now, we will show that there is two dimensional section of the basin boundary which has a fractal structure.

Let us consider a two dimensional one to one and continuous map M . We choose two sets \hat{A} and \hat{B} such that $\hat{A} \subset A$ and $\hat{B} \subset B$ where A, B are two basin sets. Of course we have $\hat{A} \cap \hat{B} = \emptyset$. We choose a test set I (gray rectangle in figure 13) and iterate $M(I)$. If $M(I)$ and I cross in the way presented in figure 13 we could say something more about structure of set I (see figure 14). There are subsets in I which go to A or B . By D we denote this part of domain for which we are not sure where it goes to. The repetition of this procedure will reveal more and more complicated structure of the test set. In the limit we will get a structure similar to a fat Cantor set.

With the help of the Poincaré map we could reduce three dimensional flow to two dimensional map (Poincaré map is one to one and continuous as map M). Test set and its intersection satisfying described conditions are presented in figure 15.

¹It will be described elsewhere.

It follows from the foregoing that there is a surface in the phase space whose intersection with the basin boundary has a fractal structure. This, together with numerical data implies existence of the chaotic solution. We believe the mathematically rigorous proof can be done by applying the method presented in [10].

8 Route to chaos

There is also a parallel description of the phenomenon presented in the previous section which helps to follow “the route to chaos” in Poincaré picture.

The system (6–8) has reflection symmetry $F \rightarrow -F$ so for each initial value of c^* also $-c^*$ gives critical solution. We take a slice of the whole phase space and we denote by N the map defined by subsequent intersections of the flow with the chosen slice. This corresponds to four period two points for small positive α (intersection of two loops with the surface). Map N^2 reduces four periodic points to two saddles and gives us proper Poincaré section. These saddles lay in the basin boundary. The intersection of the basin boundary with Poincaré surface gives stable manifolds of the saddles for N^2 . If we choose Poincaré section with $F = const$, we can use existing symmetries to determine unstable manifolds. The derivatives W', D' are invariants of the reflection $W \rightarrow -W, D \rightarrow -D$. It follows from this that stable manifolds under this transformation correspond to unstable manifolds (see figure 16). The crossings determine positions of the saddles. The shapes of the manifolds and positions of the saddles depends on the parameter α .

For small α , b -orbits have been found analytically (see [3]). We know from this three dimensional analysis that for $\alpha \rightarrow 0$ periodic solutions run towards infinity (as we can see in figure 2) and their period shrinks to zero. That means in terms of the Poincaré picture that the distance between saddles is unbounded for $\alpha \rightarrow 0$.

If we go in the opposite direction (growing α) the distance between the unstable manifold of the first saddle and the stable manifold of the second saddle decreases. At the bifurcation point they collide ($\alpha \simeq 0.426$) and the heteroclinic intersection arises (see figure 16). This implies an infinite number of intersections and a chaotic nature of C-attractor. For larger values of α ($\alpha \simeq 0.482$) the heteroclinic intersection disappears and C-attractor becomes periodic again.

The bifurcation of the basin boundary seems to be different from the one “at point” described for the Henon map. We have observed that manifolds are deformed just before bifurcation point ($\alpha = 0.4244$, figure 17). Further investigation is needed to clarify this fact.

9 Final remarks

The main result of this paper is the qualitative and quantitative argument for the existence of a chaotic solutions of the equations (1-3). We have skipped the physical background but we point out that these equations are reduced Einstein's equations. In addition, chaotic solutions separate two generic types so in this sense they are critical. As far as we know this is the first example of fractal critical behavior in the context of Einstein's equations [11].

10 Acknowledgments

I would like to express my gratitude to Piotr Bizoń for help.

The research of the author was supported in part by the KBN grant no. 2P03B00623 and in part by the FWF grant no. P15738.

References

- [1] P. Bizoń and A. Wasserman. Self-similar spherically symmetric wave maps coupled to gravity. *Physical Review D*, 62(084031), 2000.
- [2] P. Bizoń and A. Wasserman. On the existence of self-similar spherically symmetric wave maps coupled to gravity. *Class. Quantum Grav.*, 19(3309), 2002.
- [3] P. Bizoń, S. J. Szybka, and A. Wasserman. Periodic self-similar wave maps coupled to gravity. Preprint gr-qc/0310038, 2003.
- [4] S. Husa, C. Lechner, M. Pürner, J. Thornburg, and P. C. Aichelburg. Type II critical collapse of a self-gravitating nonlinear sigma models. *Phys. Rev.*, D62(104007), 2000.
- [5] S. W. McDonald, C. Grebogi, E. Ott, and J. A. Yorke. Fractal basin boundaries. *Physica*, 17D:125–153, 1985.
- [6] P. M. Battelino et al. Multiple coexisting attractors, basin boundaries and basic sets. *Physica D*, 32(296), 1988.
- [7] Helena E. Nusse and James A. Yorke. A numerical procedure for finding accessible trajectories on basin boundaries. *Nonlinearity*, 4:1183–1212, 1991.
- [8] P. Grassberger. How to measure self-generated complexity. *Physica A*, 140(319), 1986.
- [9] D. R. Moore and N. O. Weiss. Sensitivity of bifurcations to discretization. *Inst. Math. Appl. Conf. Ser. New Ser.*, 34:107–125, 1992.
- [10] K. Mischaikow, M. Mrozek, and A. Szymczak. Chaos in the Lorenz equations: A computer assisted proof - part III: Classical parameter values. *J. Differ. Equ.*, 169(1):17–56, 2001.
- [11] C. Gundlach. Critical phenomena in gravitational collapse. *Phys. Rept.*, 376:339–405, 2003. Preprint gr-qc/0210101.

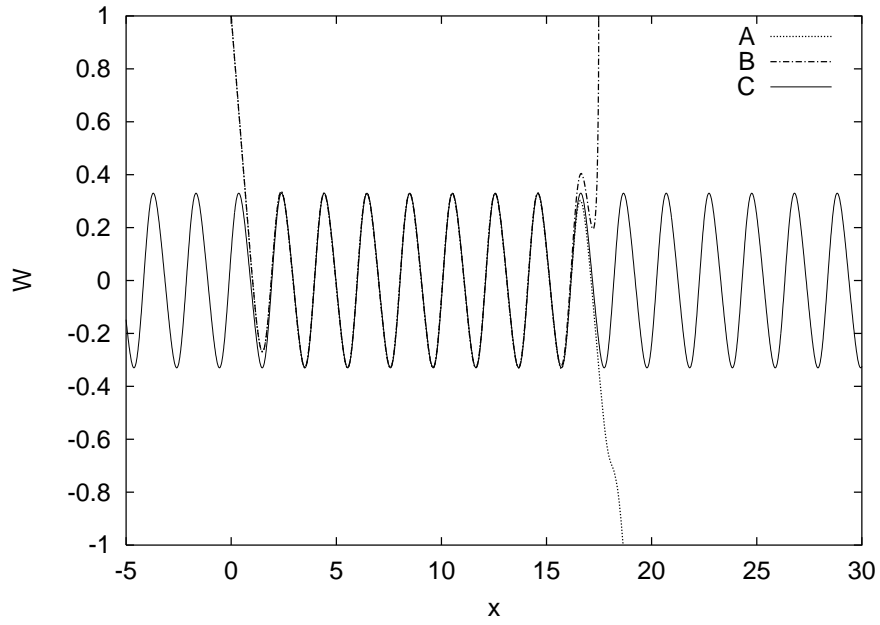


Figure 1: The function W - the type C solution (periodic). The type A solution ($c = 2.36134$), the type B solution ($c = 2.36135$). All calculations for $\alpha = 0.38$. The type A, B solutions follow periodic C-attractor for some time and then run towards A and B attractor.

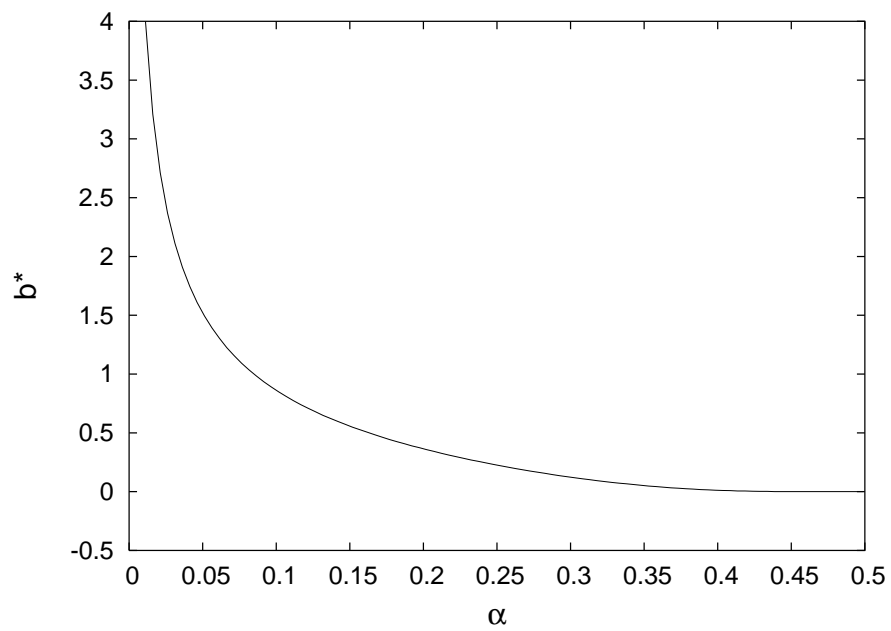


Figure 2: The bifurcation diagram, lattice $\Delta\alpha = 10^{-3}$ i $\Delta b = 2 \cdot 10^{-3}$. The critical curve $b^*(\alpha)$ separates type A solutions from type B solutions.

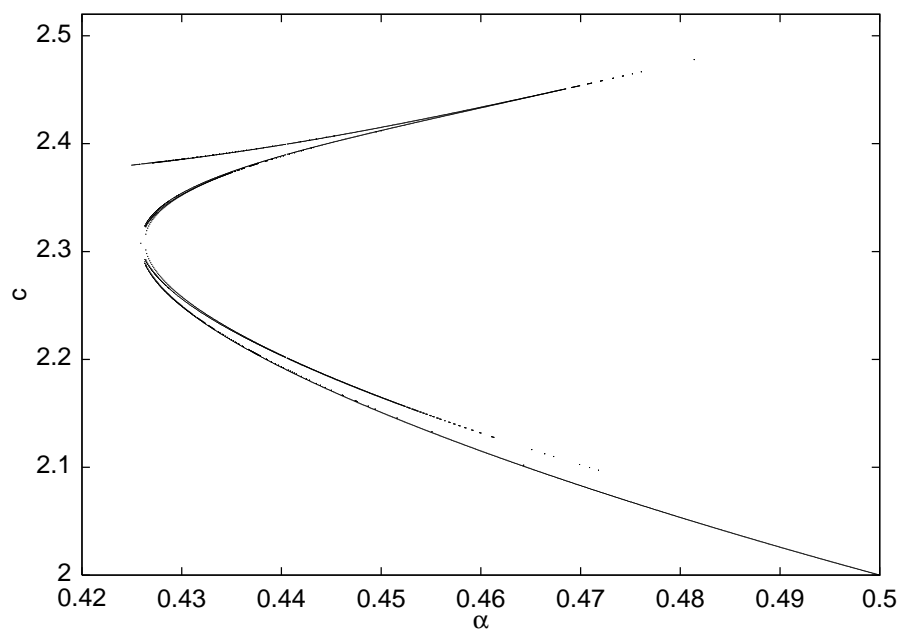


Figure 3: The bifurcation diagram, lattice $\Delta\alpha = 10^{-4}$ i $\Delta c = 2 \cdot 10^{-4}$. The critical curve $c(\alpha)$ separates type A solutions from type B solutions.

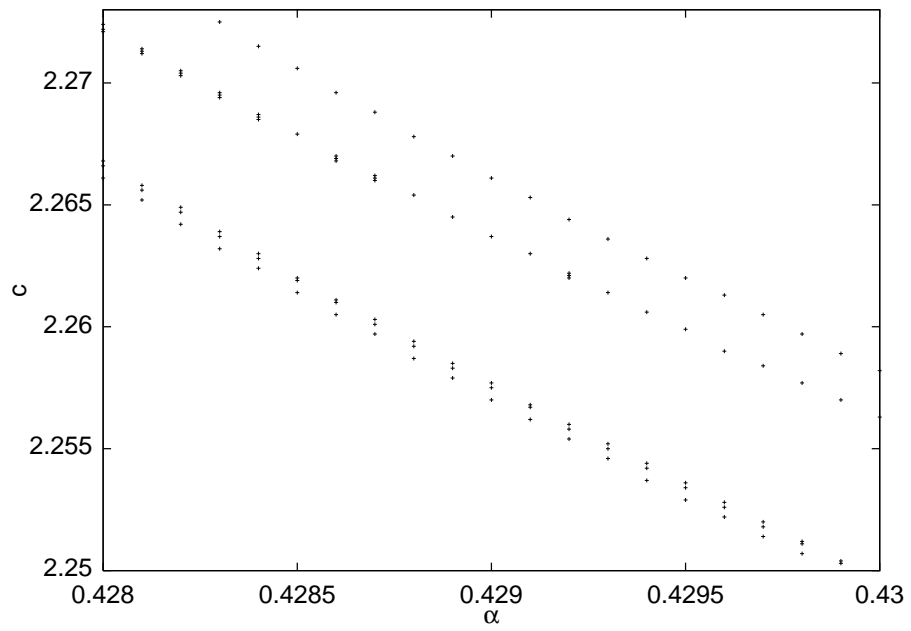


Figure 4: The bifurcation diagram (figure 3) enlarged 1000 times , lattice $\Delta\alpha = 10^{-4}$ and $\Delta c = 2 \cdot 10^{-4}$. The complex structure of the basin boundary is visible.

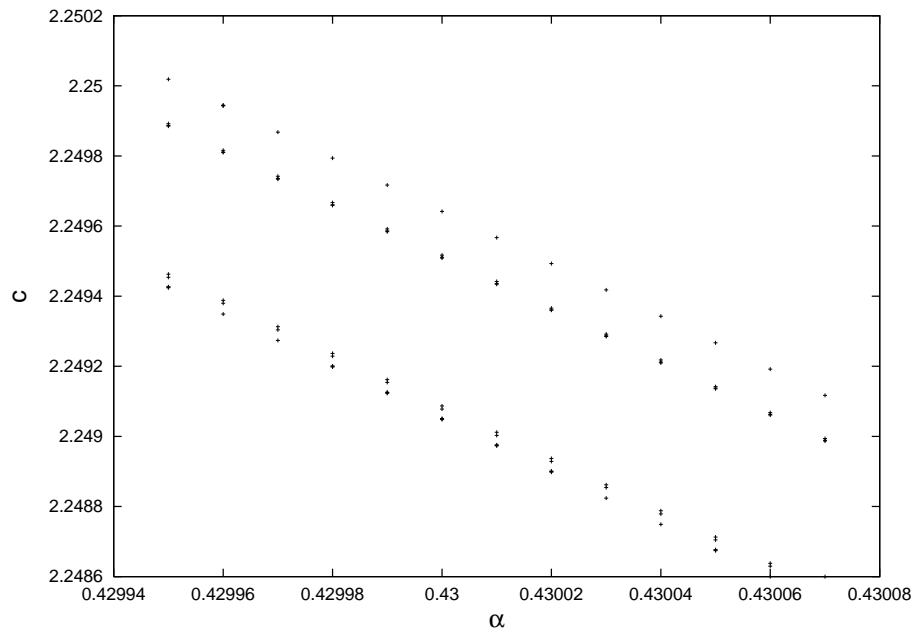


Figure 5: The bifurcation diagram (figure 3) enlarged 200000 times, lattice $\Delta\alpha = 10^{-5}$ i $\Delta b = 10^{-6}$. The complex structure of the basin boundary is visible.

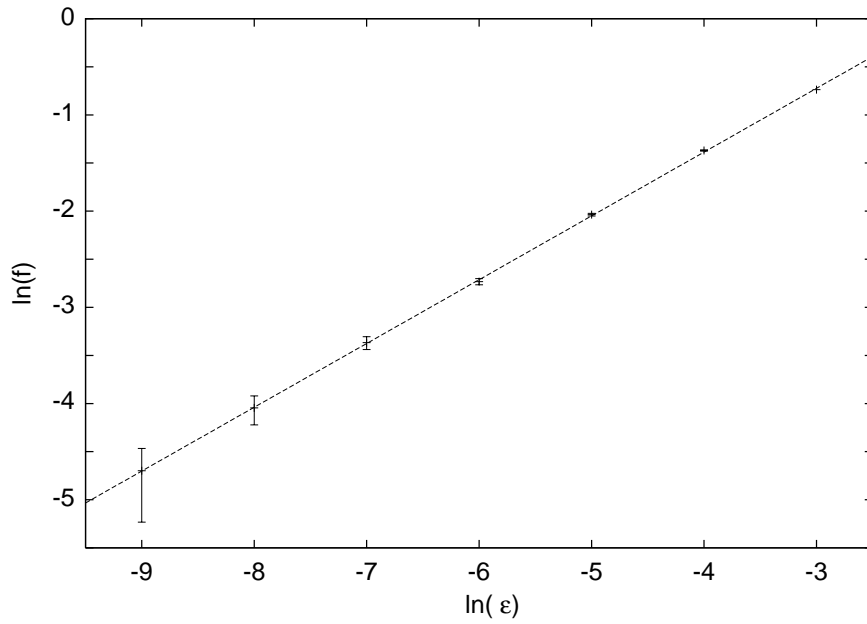


Figure 6: The number of uncertain points in the phase space (for $\alpha = 0.4264$) as a function of the perturbation parameter ϵ (logarithmic scale). The linear fit gives the slope $a = 0.663 \pm 0.003$ from which using (12) and (13) we get the capacity dimension $d = 0.337 \pm 0.003$.

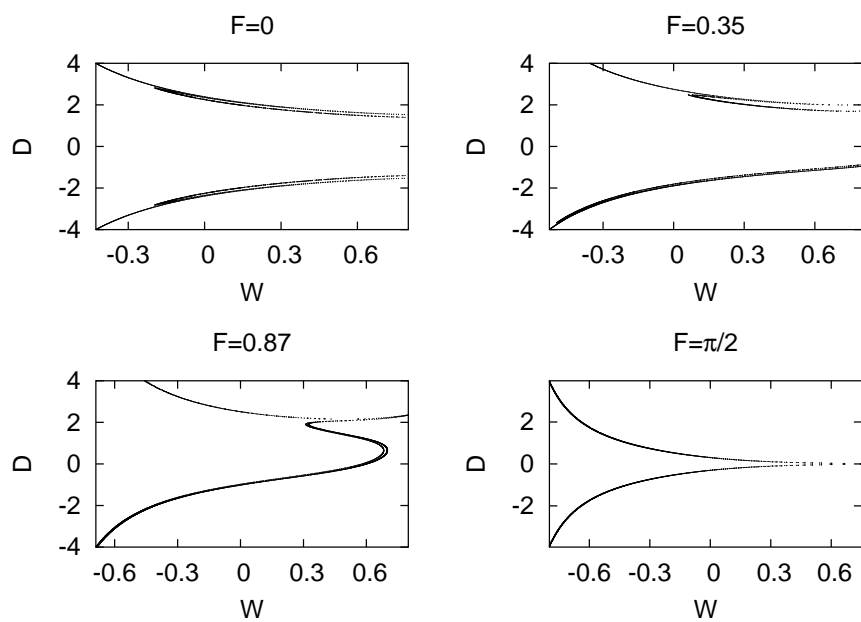


Figure 7: The basin boundary for $\alpha = 0.43$. The complex structure is visible.

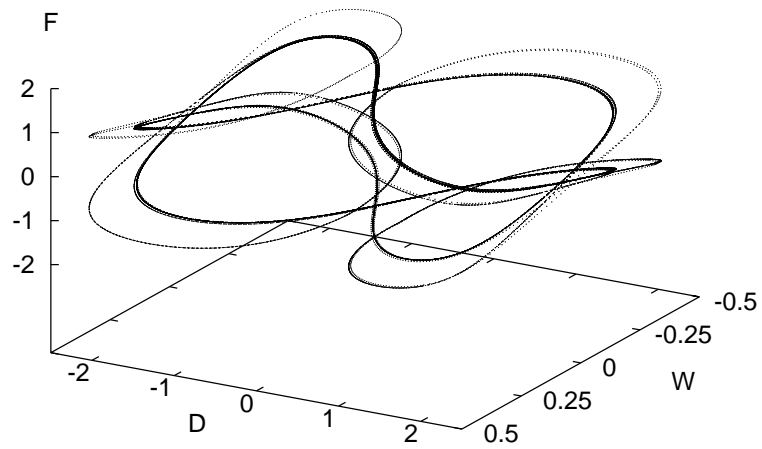


Figure 8: C-attractor in phase space (W, D, F) (for F we identify the intervals $[-\frac{\pi}{2} + \pi k, \frac{\pi}{2} + \pi k]$ where $k \in \mathbb{N}$), $\alpha = 0.43$.

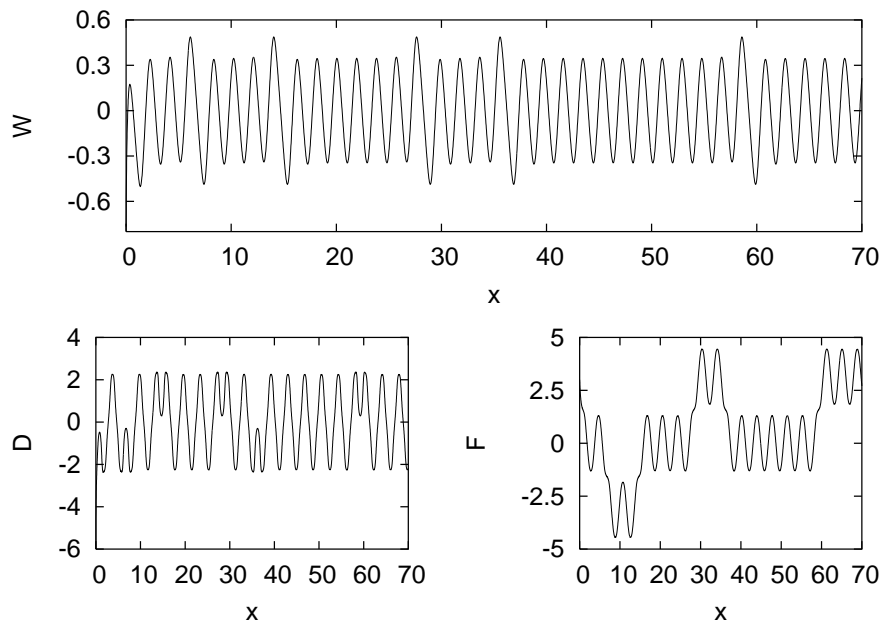


Figure 9: The typical solution on C-attractor, $\alpha = 0.43$

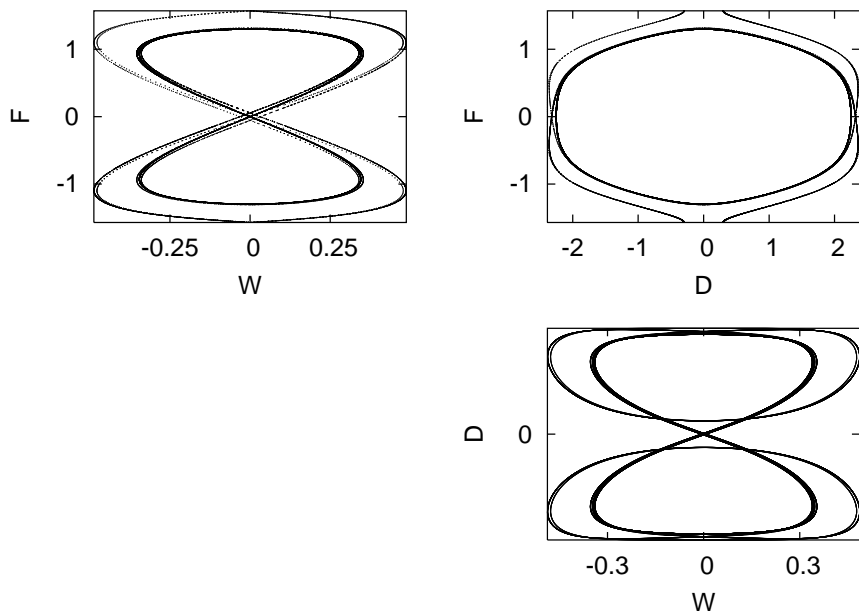


Figure 10: The projection of C-attractor, $\alpha = 0.43$ (for F we identify the intervals $[-\frac{\pi}{2} + \pi k, \frac{\pi}{2} + \pi k]$ where $k \in \mathbb{N}$). Some similarities to the Lorenz attractor are visible.

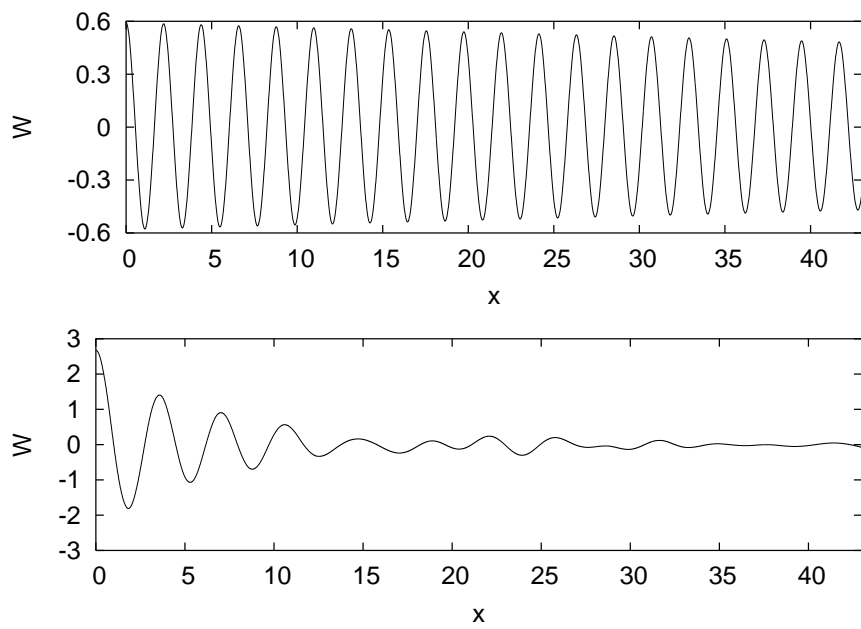


Figure 11: The correlation function; the comparison of the periodic solution $\alpha = 0.42$ with chaotic $\alpha = 0.43$ (only short time correlation exist).

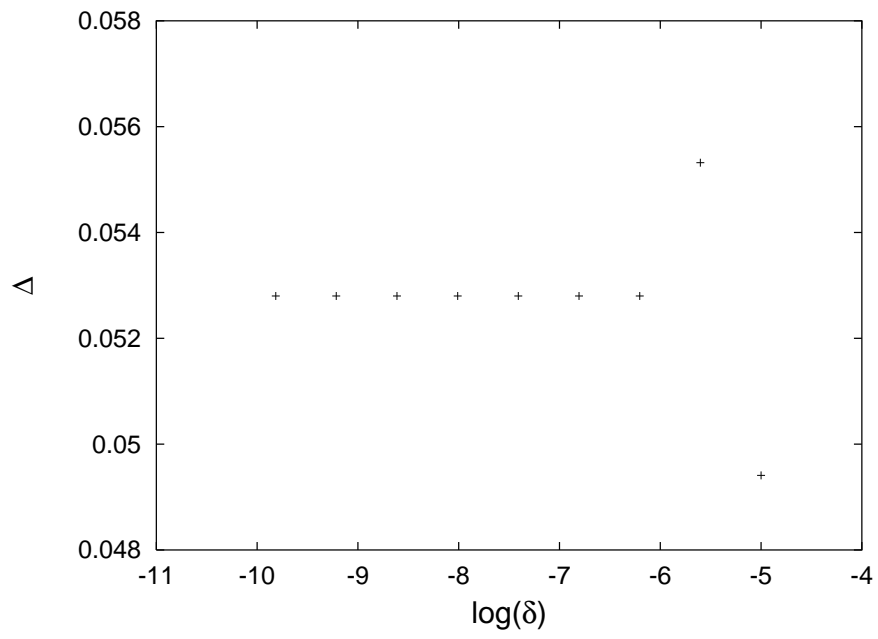


Figure 12: The size of chaotic window as a function of the numerical precision. Since the result does not tend to zero with increasing machine precision we believe that the observed chaotic behavior is not a numerical artifact.

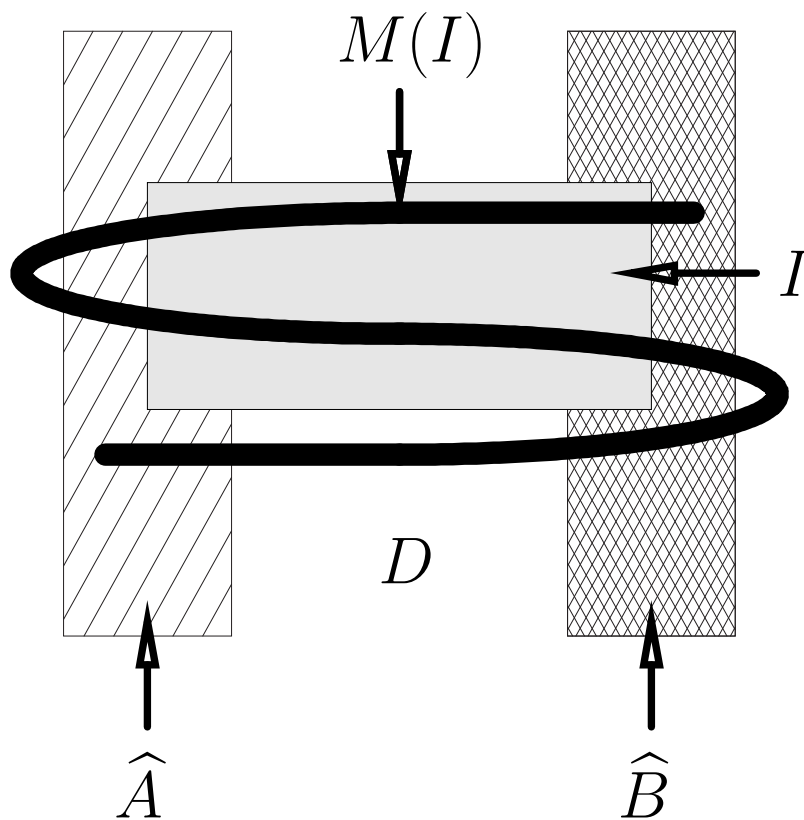


Figure 13: Sets: \widehat{A} , \widehat{B} , test set I and $M(I)$ (S-shape). We have: $\widehat{A} \subset A$ and $\widehat{B} \subset B$ where A, B are two basin sets. The horseshoe in the crossing $M(I)$ and I signals fractal boundary between A and B .

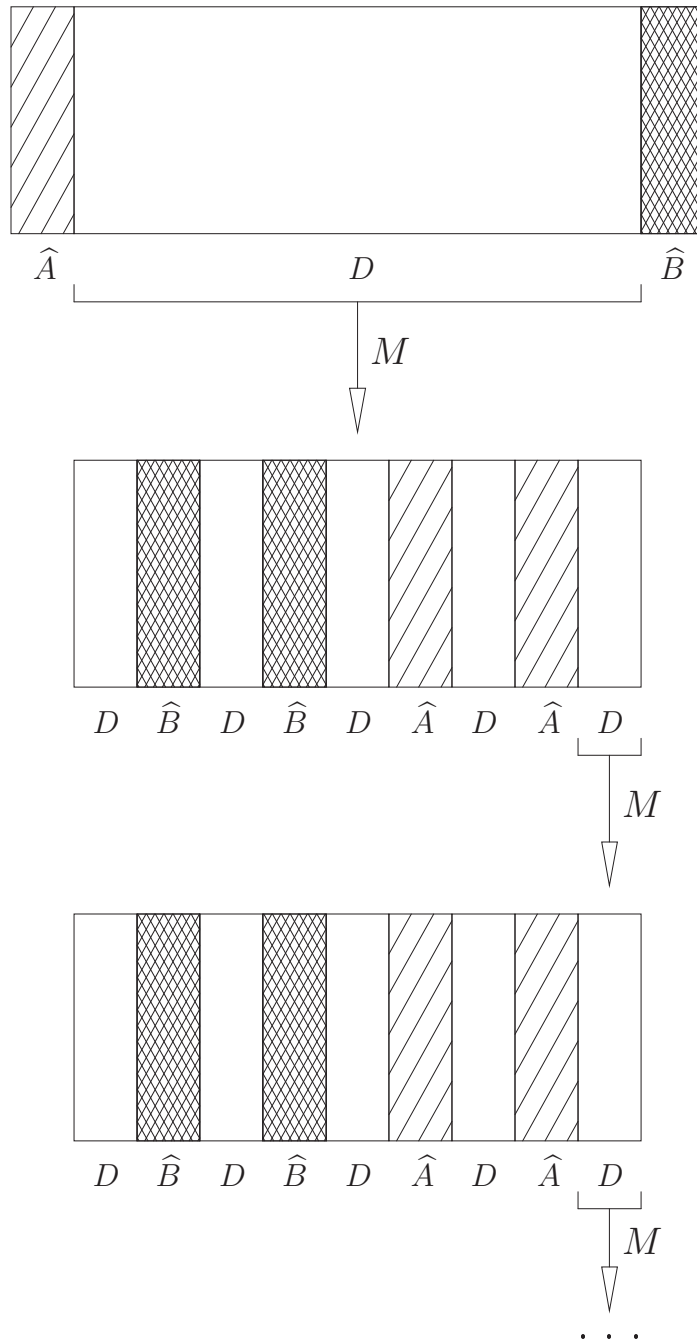


Figure 14: The structure of the set I determined after 0, 1, 2 iterations of the map M . The repetitions of this procedure converge to a part of the boundary (between basin sets A and B) and will lead to a fat Cantor set in the limit.

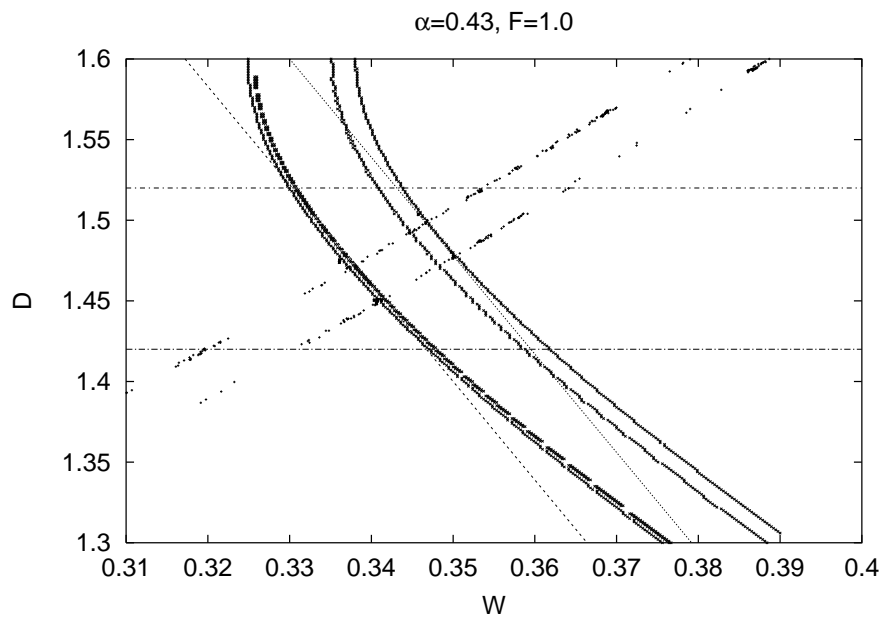


Figure 15: The intersection of the test set I (bounded by straight lines) and its first image by Poincaré map. We have plotted in the background the basin boundary (visible as four, almost parallel curves). These curves correspond to the stable manifolds of the periodic points. The first iteration of the test set I corresponds to the unstable manifolds. We observe horseshoe as in figure 13. This is a “first approximation” of the heteroclinic intersection (figure 16).

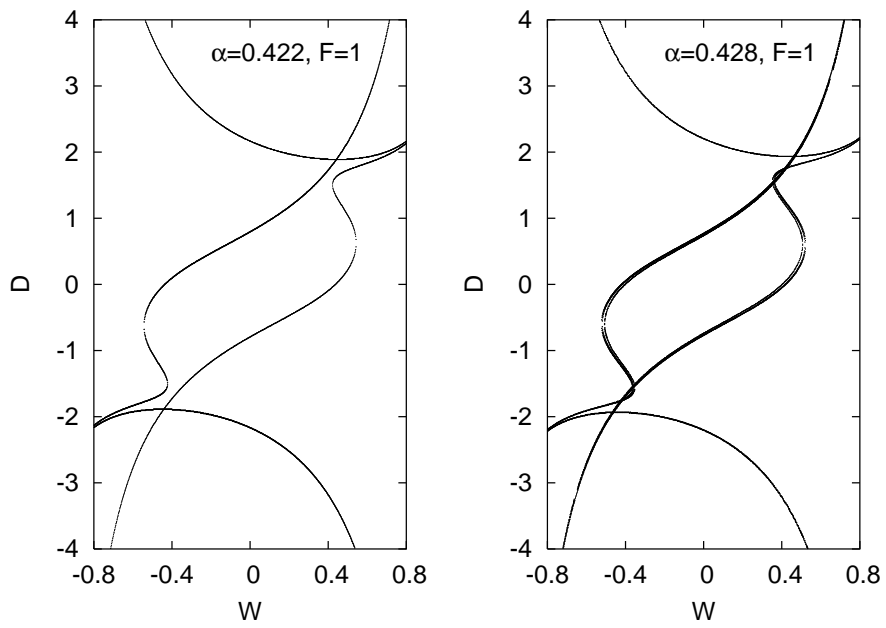


Figure 16: Two saddles and the creation of the heteroclinic intersections of stable and unstable manifolds.

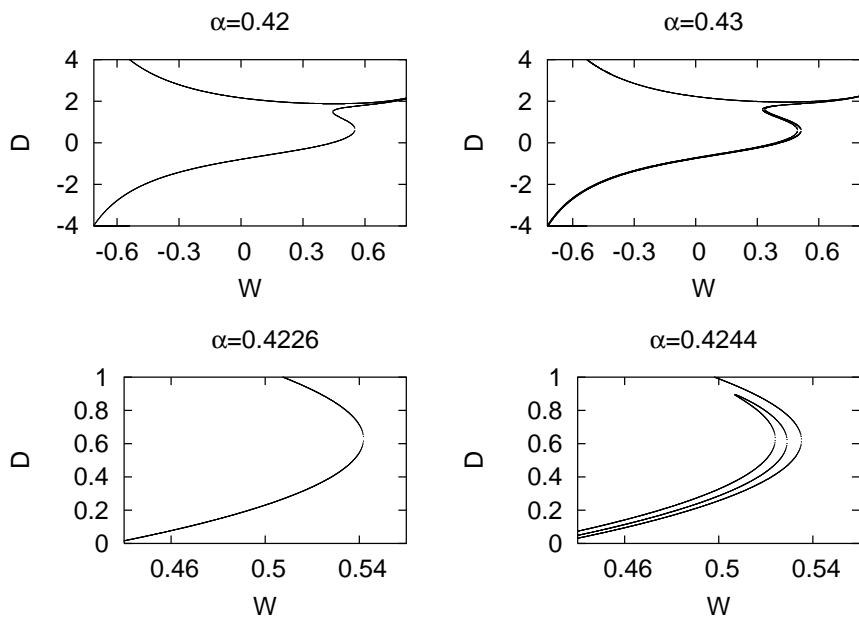


Figure 17: The bifurcation of the basin boundary, $F=1.0$. The strong deformation is observed ($\alpha = 0.4244$) before a chaotic behavior appears ($\alpha \simeq 0.426$).